Array Location Uncertainty in Imaging Radar: SAR vs. MIMO-SAR

Babak Mamandipoor, Thomas Teisberg, Siavash Kananian, Amin Arbabian
EE Department, Stanford University, Stanford, CA 94305
Email: bmamandi@stanford.edu

***Abstract*—In this paper, we consider a type of MIMO-SAR architecture in which the elements are arranged along the axis of platform motion. We show that this architecture can be used to improve the robustness and accuracy of angular estimation compared to single-element SAR given array location uncertainty. We compare three different architectures for side-looking radars (SAR, SIMO, and SIMO-SAR) and show that in the presence of array location uncertainty, SIMO-SAR proves more resilient. Measurement results using a commercial automotive radar module have been performed to verify this effect.**

***Index Terms*—Radar, SAR Imaging, MIMO Radar, Array Location Uncertainty, MIMO-SAR Radar, Automotive Radar.**

I. Introduction

The use of radar sensors is growing rapidly in a wide range of applications including automotive, unmanned aerial vehicles, industrial, and more. Radar achieves better performance at a lower cost, especially in adverse weather conditions, compared to LiDAR, IR cameras, or visible cameras [1] and will play a crucial role in realizing future autonomous driving [2] and drone navigation and situational awareness systems [3]. Currently, many vehicles are equipped with radar-based comfort and safety systems, such as adaptive cruise control and automatic emergency braking. However, emerging applications of imaging radar, which enable situational awareness, navigation, collision avoidance, etc., call for better angular and range resolution as well as a larger field of view compared to the state-of-the-art sensors.

Recent advances in silicon integrated circuit technologies has enabled high performance systems in mm-wave frequencies with higher levels of integration at lower cost, and smaller size [4], [5]. Moreover, large swathes of bandwidth available at mm-wave frequencies (e.g., 5 GHz of spectrum from 76 to 81 GHz for automotive applications [6]) along with smaller wavelength (compared to the aperture size), lead to a significant improvement in range and angular resolution, respectively. A pragmatic approach for increasing the aperture size, and hence improving the angular resolution of an imaging radar, is by moving the antenna elements in space and synthesizing a large virtual aperture. This technique is known as Synthetic Aperture Radar (SAR), and has been widely implemented especially for airborne imaging applications [7] and, more recently, for automotive radar applications [8]. SAR requires platforms that are stable to within a fraction of the wavelength or whose location can be reliably and accurately characterized [9]. In [10], it is shown that platform location uncertainty in automotive radar causes defocussing in range-azimuth plots and a motion compensation technique based on accurate estimation of radar location is employed to suppress this effect.

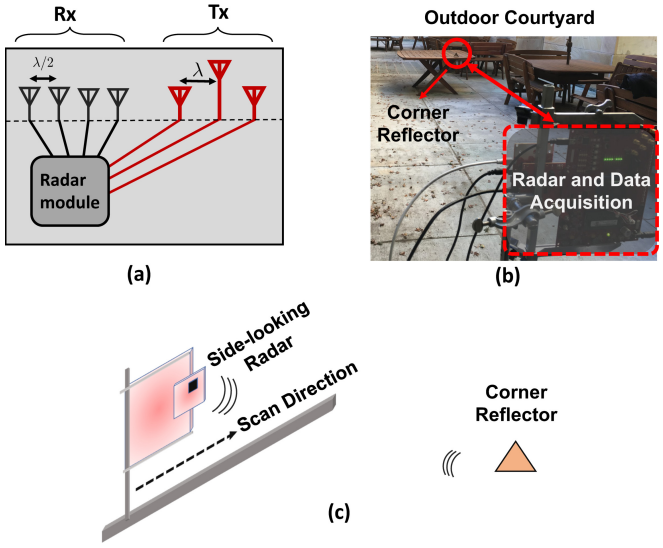

Fig. 1. a) Antenna arrangement in TI's AWR1243 radar module, b) measurement setup in an open courtyard with a corner reflector in the scene, c) the radar platform mounted on a linear stage with the possibility of creating a large virtual aperture by spatial scanning.

Antenna location uncertainty, in the form of small vibrations of the radar platform, has also been studied in the literature. For instance, [11] and [12] have shown that vibrations in automotive radar result in ambiguous detection of moving versus stationary targets, ghost targets, and spurious Doppler components due to the disturbance of the phase information in the received signals.

Multiple-input-multiple-output (MIMO) techniques have been combined with SAR to synthesize a 2D array based on scanning a 1D MIMO array perpendicular to the axis of the elements. In this context, MIMO-SAR offers spatial diversity, resolution improvement, and 3D imaging [13], [14]. In this paper, we consider a different type of MIMO-SAR architecture where the elements are arranged along the axis of motion. While this does not enable 3D imaging, we show that it can be used to improve the angular estimation compared to single-element SAR given array location uncertainty. This architecture could also be combined with additional elements

978-1-5386-1725-0/18/$31.00 ©2018 IEEE

TABLE I
WAVEFORM PARAMETERS USED FOR EXPERIMENTS.

Parameter	Value
Carrier frequency	77 GHz
Chirp bandwidth (BW)	1.875 GHz
Chirp duration	71.4 μsec
Pulse repetition interval	94.3 msec
ADC sampling rate	7.171 MSample/sec
Speed of linear stage	1.03 cm/sec

in the perpendicular axis to add 3D imaging capabilities. We consider three different architectures for side-looking radars, namely SAR, SIMO, and SIMO-SAR, and investigate their angular estimation accuracy and robustness in the presence of inevitable array location uncertainty. Measurement results using a commercial automotive radar module are presented.

II. RADAR PLATFORM

For radar measurements, Texas Instrument's 76-to-81GHz automotive radar sensor evaluation module (AWR1243BOOST)[1] is used along with a debug add-on board and data acquisition module. The radar module is comprised of three transmitter (Tx) and four receiver (Rx) elements (as depicted in Fig. 1a), and is capable of collecting MIMO measurements by time division multiplexing (TDM) across the three transmitters. For the measurements reported in this paper, we only use one Tx element for illuminating the scene, while all of the four Rx elements are used to collect the back-scattered electromagnetic waves. The radar is placed in an open courtyard (Fig. 1b) with a corner reflector located at a range of ~ 5.7 meters and azimuth angle of $\sim 14^\circ$ to the left from boresight. As conceptually depicted in Fig. 1c, the radar module is mounted on a Zaber linear stage to provide SAR functionality by scanning across a line, hence creating a large virtual aperture. The radar transmits a sequence of chirps, also known as linear Frequency Modulated Continuous Wave (FMCW) signals. Waveform parameters are set according to Table I. Range resolution is given by $\delta r = \frac{c}{2BW} \approx 8$ cm, where c is the speed of light, and BW is the bandwidth of the chirp waveform.

III. SIGNAL PROCESSING AND ACQUISITION MODEL

In this section, we first provide an overview of the signal processing technique that we have used for extracting range-angle information for any point target in scene. Then we briefly describe the radar architectures that have been used for collecting the measurement data.

A. Signal Processing Overview

The data acquisition parameters for the radar module and the linear stage are set such that the *effective array* corresponding to any of the radar architectures considered in this paper, forms a uniform linear array with $\lambda/2$ spacing between the elements, where λ is the wavelength. This ensures a fair comparison

[1]See: http://www.ti.com/tool/AWR1243BOOST.

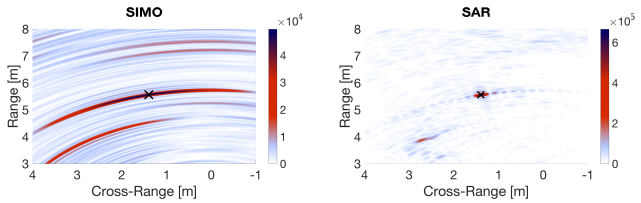

Fig. 2. A comparison of the range-angle plots for SIMO with four physical elements (left) versus a much larger synthetic aperture with N = 56 virtual element (right). The black cross represents the true target location.

of the performance and robustness for different architectures with the same number of effective array elements. Moreover, a unified signal processing algorithm can be applied to the data acquired by different architectures to extract range-angle information. Here, we use a digital beamforming algorithm to process the data, by first taking a Fourier transform in fast time (i.e., duration of each chirp) to extract the beat frequencies and the corresponding range information (range compression), followed by a matched azimuth filter across the virtual array elements to extract the azimuth angle of the scatterers in the scene. The fast time Fourier transform has been implemented using Fast Fourier Transform (FFT) to speed up processing, whereas the matched azimuth filter is implemented for a uniform grid over the azimuth angles, which results in a non-uniform Fourier transform across the array elements.

In order to verify the performance of our signal processing algorithm as well as the capability of our measurement setup to exploit the SAR data for enhancing the angular estimation accuracy, we first analyze the 3 dB azimuth beamwidth corresponding to the corner reflector in the scene for various number of virtual array elements. Fig. 2 shows an example of the range-angle plots corresponding to SIMO (with 4 physical Rx elements), and SAR (with 56 virtual array elements). We see a significant enhancement in the cross-range resolution of the SAR architecture. As the number of elements used in the reconstruction increases, the 3 dB width of the detection from a point target decreases. For a theoretical point target and N isotropic anetnna elements with $\lambda/2$ spacing, the 3 dB width is approximately described by $2.412/N$ (in radians), following a similar derivation to the one given by [15]. Fig. 3 shows that the result of our measurement data constructed with an increasing number of elements corresponds well to this theoretical quantity.

B. Array Architectures

In this subsection, we briefly describe different array architectures used for collecting the measurement data. From a single set of data, we assemble a full $\lambda/2$ spacing virtual array with N = 56 elements, hence constructing an aperture of size ~ 11 cm. Using this same set of data, we post-process the data differently to simulate a single physical element SAR configuration or a SIMO-SAR configuration with four physical elements.

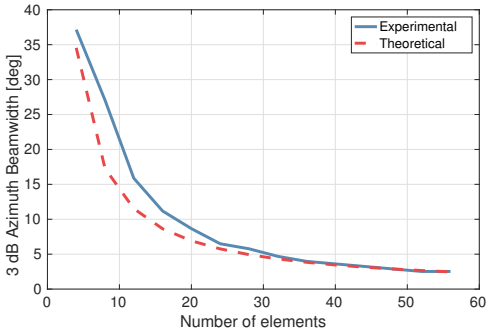

Fig. 3. Comparison between theoretical and experimental results for the 3 dB azimuth beamwidth of a corner reflector with an increasing number of elements in the synthetic aperture.

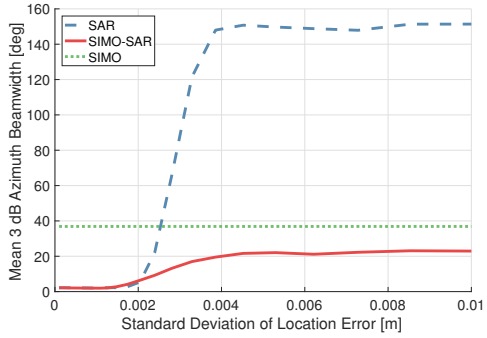

Fig. 4. Mean of the 3 dB azimuth beamwidth of the detected corner reflector as a function of the standard deviation of uniformly distributed errors in the array location information.

1) SAR: In this configuration, we construct a large virtual aperture with the movement of a single pair of transmit and receive antenna. This single pair is used to assemble a $\lambda/2$ array by transmitting chirps in uniform time intervals. Movement of the radar platform induces some uncertainty in the location of the antenna at the time of each chirp. We assume that platform velocity is slow enough that the radar can be considered stationary for the duration of a single chirp. To simulate the effect of array location uncertainty for this architecture, we add independent and uniformly distributed errors to the location estimate of each element in the virtual array.

2) SIMO-SAR: As described previously, our radar module is comprised of four Rx antenna elements arranged along the axis of the platform motion. For SIMO-SAR configuration, we use a single Tx to illuminate the scene, and all four Rx elements to capture the back-scattered data. This measurement process combined with the motion of the platform is used to construct a large virtual aperture. We again assume that the platform velocity is slow enough that the radar can be considered stationary for the duration of a single chirp. In this architecture, the precise spacing between the physical antennas within the module is known, but the location of the entire module has some uncertainty as a result of the platform motion. Thus, we assume that sets of four receive elements (comprising a module) remain fixed relative to each other, but there is uncertainty in the estimation of the locations of these sets relative to each other. This uncertainty has been modeled by introducing independent and uniformly distributed errors in the location of the sets.

3) SIMO: As a benchmark, we also consider a SIMO architecture using only a single module of four physical Rx elements. Note that the relative locations of the Rx elements are known and fixed. There may still be uncertainty in the location of the total array, however this has minimal effect on the estimation of obstacles. It is important to note that this configuration does not take advantage of the motion of the platform in any way and also can be expected to have far lower angular resolution as a result of having far fewer antenna elements.

IV. Experimental Results

A. Experiment Setup

To evaluate angular estimation error, we have collected measurements in an open courtyard with a single corner reflector acting as a point target, as depicted in Fig. 1. The target is at a range of approximately 5.7 meters from the radar and at about 14° to the left from boresight.

In the following experiments, we used the data collected and subsampled to form a virtual uniform array of $N = 56$ elements. We added independent and uniformly distributed errors with increasing standard deviation to either the module location or the element location, a described in Section III-B. We used a maximum likelihood estimate of the object parameters (assuming additive white Gaussian noise across time and antenna elements), given by maximum peak in the constructed range-angle matrix to quantify the estimation performance of different architectures. We have also considered the 3 dB azimuth beamwidth as defined by the extent of angular bins in the identified range bin having a value over half the maximum value to evaluate the resolution degradation as a result of array location uncertainty. Since we assume a single point target in the scene, this includes all bins over the 3 dB point, even if they are separated from the maximum peak. Lastly, detected peaks with a range of less than 0.2 meters from the radar platform were filtered out.

B. Azimuth Angular Resolution

The 3 dB azimuth beamwidth, as described above, is shown in Fig. 4 for all three architectures. First, consider the SIMO case relative to SAR or SIMO-SAR at zero location error. As is well known, increasing the number of elements will increase the angular resolution, thus the architectures with larger virtual arrays have a much smaller 3 dB extent than the SIMO case with only 4 elements. This effect is shown by the comparison between a 4-element SIMO and a large synthetic aperture in Fig. 2. Note that SAR and SIMO-SAR are equivalent if there is no error in the array location information. As the noise increases, the 3 dB region for the SAR architecture grows rapidly and converges to a range of about 150°. With

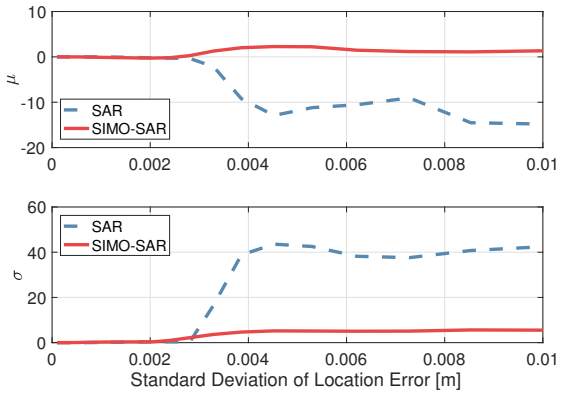

Fig. 5. Mean μ (top) and standard deviation σ (bottom) of the distribution of the error in azimuth angle estimation.

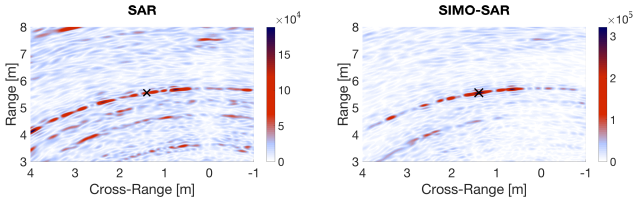

Fig. 6. Example range-angle plots with uniformly distributed error of 1cm standard deviation added to the array location information. The black cross is the true location of the target.

a 3 dB range of 150°, there is effectively no useful angular information in the detection.

The SIMO-SAR architecture behaves differently. As a result of 4-element groups having known locations, the extent of the 3 dB region grows much more slowly. Even as the location noise becomes very large, is stabilizes below the level of the SIMO case. This behavior indicates that SIMO-SAR is capable of maintaining the benefits of an increased aperture size compared to SIMO even in the presence of module location uncertainty. Note that for the experiments reported in this paper, the variation of the azimuth angle of arrival of the reflections from the corner reflector across the virtual aperture is very small. The effect of array location uncertainty for a much larger aperture where different array elements see the target from a different vantage point (hence, a different azimuth angle) is out of the scope of this paper.

The mean μ and standard deviation σ of the distributions of angular estimation errors are compared in Fig. 5. As expected, the mean error and standard deviation are very close to zero for both architectures under the low location error cases. As the introduced error increases, a significant bias appears in the SAR architecture. While the SIMO-SAR mean error does shift noticeably, it stays within a few degrees of zero, even at very large location uncertainty. The standard deviation of the estimation error also levels out at about 5°, far better than the roughly 40° standard deviation of the SAR case.

The selected range-angle plots shown in Fig. 6 are characteristic of the behavior of each architecture. The SAR architecture tends to have little discernible structure left once array location uncertainty is introduced. The detections can fall over a broad range of angles and have little correlation with the true target. In the SIMO-SAR case, however, the peaks tend to be close to the true target, even if they shift by some amount as a result of the location errors.

V. Conclusion

We have investigated the effect of array location uncertainty in estimating the spatial location of a point target using an array of antenna elements. Three different architectures for constructing the aperture have been considered. We have shown that constructing a large virtual aperture by spatial scanning of a MIMO (or SIMO) physical array of antenna elements arranged along the direction of motion leads to a significant improvement in the robustness and accuracy of the angular estimates compared to a SAR architecture with the same number of effective elements constructed by spatial scanning of a single pair of Tx/Rx elements.

Acknowledgment

The authors would like to thank Texas Instruments for support of this work and providing the hardware platform.

References

[1] S. M. Patole and et al., "Automotive radars: A review of signal processing techniques," *IEEE Signal Process. Mag.*, vol. 34, no. 2, pp. 22–35, March 2017.
[2] J. Hasch, "Driving towards 2020: Automotive radar technology trends," in *Proc. Int. Conf. Microw. for Intell. Mobility*, April 2015, pp. 1–4.
[3] M. Schuetz and et al., "A custom lightweight UAV for radar remote sensing: Concept design, properties and possible applications," in *Proc. Int. Conf. Microw. for Intell. Mobility*, March 2017, pp. 107–110.
[4] E. Ozturk and et al., "Measuring target range and velocity: Developments in chip, antenna, and packaging technologies for 60-GHz and 122-GHz industrial radars," *IEEE Microw. Mag.*, vol. 18, no. 7, pp. 26–39, Nov 2017.
[5] T. Zwick and et al., "Pea-sized mmW transceivers: QFN-based packaging concepts for millimeter-wave transceivers," *IEEE Microw. Mag.*, vol. 18, no. 6, pp. 79–89, Sept 2017.
[6] *Federal Communications Commission, Radar Services in the 76-81 GHz Band, ET Docket No. 15-26*, 2017.
[7] J. P. Fitch, *Synthetic aperture radar*. New York: Springer, 1988.
[8] R. Feger and et al., "Experimental verification of a 77-GHz synthetic aperture radar system for automotive applications," in *Proc. Int. Conf. Microw. for Intell. Mobility*, March 2017, pp. 111–114.
[9] J. T. Richard and H. O. Everitt, "Millimeter wave and terahertz synthetic aperture radar for locating metallic scatterers embedded in scattering media," *IEEE Trans. THz Sci. Technol.*, vol. 7, no. 6, pp. 732–740, Nov 2017.
[10] H. Wu and T. Zwick, "A novel motion compensation algorithm for automotive SAR : Simulations and experiments," in *Proc. German Microw. Conf.*, March 2010, pp. 222–226.
[11] F. Hau and et al., "Influence of vibrations on the signals of automotive integrated radar sensors," in *Proc. Int. Conf. Microw. for Intell. Mobility*, March 2017, pp. 159–162.
[12] M. Harter and J. Hildebrandt, "Vibrations in automotive radar systems," in *Proc. Int. Conf. Microw. for Intell. Mobility*, May 2016, pp. 1–4.
[13] W. Q. Wang, "MIMO SAR imaging: Potential and challenges," *IEEE Aerosp. Electron. Syst. Mag.*, vol. 28, no. 8, pp. 18–23, Aug 2013.
[14] D. Oppelt and et al., "MIMO-SAR based millimeter-wave imaging for contactless assessment of burned skin," in *Proc. IEEE Int. Microw. Symp*, June 2017, pp. 1383–1386.
[15] R. C. Hansen, *Phased array antennas*. Hoboken, NJ: Wiley, 2009.